Showcasing research from the laboratory of Professor Gyeong S. Hwang at the University of Texas at Austin.

Title: Reaction mechanisms of aqueous monoethanolamine with carbon dioxide: a combined quantum chemical and molecular dynamics study

Molecular mechanisms underlying the reaction of aqueous MEA with CO_2 are examined using *ab initio* and classical molecular dynamics simulations combined with static quantum chemical calculations, with special attention to the influence of solvent structure and dynamics. This work highlights the critical role of H_2O molecules, particularly their availability and arrangement around zwitterionic intermediates, in the progression of competing CO_2 capture and solvent regeneration processes. This improved understanding can contribute to developing more comprehensive kinetic models for use in modeling and optimizing the CO_2 capture process.

As featured in:

See Gyeong S. Hwang *et al.*, *Phys. Chem. Chem. Phys.*, 2015, **17**, 831.

ROYAL SOCIETY OF **CHEMISTRY**

www.rsc.org/pccp

PCCP

CrossMark
← click for updates

Reaction mechanisms of aqueous monoethanolamine with carbon dioxide: a combined quantum chemical and molecular dynamics study†

Gyeong S. Hwang,*[ab] Haley M. Stowe,[b] Eunsu Paek[a] and Dhivya Manogaran[c]

Aqueous monoethanolamine (MEA) has been extensively studied as a solvent for CO_2 capture, yet the underlying reaction mechanisms are still not fully understood. Combined *ab initio* and classical molecular dynamics simulations were performed to revisit and identify key elementary reactions and intermediates in 25−30 wt% aqueous MEA with CO_2, by explicitly taking into account the structural and dynamic effects. Using static quantum chemical calculations, we also analyzed in more detail the fundamental interactions involved in the MEA−CO_2 reaction. We find that both the CO_2 capture by MEA and solvent regeneration follow a zwitterion-mediated two-step mechanism; from the zwitterionic intermediate, the relative probability between deprotonation (carbamate formation) and CO_2 removal (MEA regeneration) tends to be determined largely by the interaction between the zwitterion and neighboring H_2O molecules. In addition, our calculations clearly demonstrate that proton transfer in the MEA−CO_2−H_2O solution primarily occurs through H-bonded water bridges, and thus the availability and arrangement of H_2O molecules also directly impacts the protonation and/or deprotonation of MEA and its derivatives. This improved understanding should contribute to developing more comprehensive kinetic models for use in modeling and optimizing the CO_2 capture process. Moreover, this work highlights the importance of a detailed atomic-level description of the solution structure and dynamics in order to better understand molecular mechanisms underlying the reaction of CO_2 with aqueous amines.

I. Introduction

The ever-increasing rate of carbon dioxide (CO_2) emissions, mainly as a result of growing fossil fuel consumption, has become a widespread concern.[1] At present, aqueous alkanolamine solvents are the predominantly used method to remove CO_2 from flue gas and natural gas.[2,3] Particularly, monoethanolamine (MEA) has been the most extensively studied for decades and is commonly used as the benchmark solvent.[2,4–6] However, scaling up of the aqueous

ᵃ Department of Chemical Engineering, University of Texas at Austin, Austin, Texas 78712, USA. E-mail: gshwang@che.utexas.edu

ᵇ Materials Science and Engineering Program, University of Texas at Austin, Austin, Texas 78712, USA

ᶜ Departments of Chemistry and Biochemistry, University of Texas at Austin, Austin, Texas 78712, USA

† Electronic supplementary information (ESI) available: Additional available content includes the energy profiles of the AIMD simulations used to calculate ΔE_{rxn} (Fig. S1). Also provided are illustrations of the various configurations considered in the proton binding energy calculations as reported in Fig. 4 (Fig. S2) and the predicted lower-barrier pathway for deprotonation from a zwitterion into a well-connected water network (Fig. S3) and to a nearby MEA molecule (Fig. S4). The functional forms and parameters of the force fields used in the CMD simulations for MEA and its derivatives are also included. See DOI: 10.1039/c4cp04518a

MEA system for commercial-scale applications tends to be impeded by MEA degradation, corrosion problems, and moreover the high parasitic energy consumption during solvent regeneration.[2,4,7] Several experimental and modeling studies have been undertaken to better understand the CO_2 capture process with aqueous MEA, but some fundamental aspects of the MEA–CO_2 reaction in an aqueous solution, particularly the role of water molecules, still remain uncertain despite its importance in designing more efficient MEA-based solvents and processes.

It has been thought that two MEA molecules react with one CO_2 molecule to form carbamate and protonated MEA, perhaps *via* a single-step termolecular (direct) or two-step zwitterion mechanism. The two-step process involves the formation of a zwitterion as an intermediate which undergoes deprotonation by another MEA to form carbamate and protonated MEA.[8,9] The single-step mechanism assumes that amine, CO_2, and base molecules form a loosely-bound complex, rather than a zwitterion, which breaks up to form the products.[10] Although recently the zwitterion mechanism is commonly adopted to explain the MEA–CO_2 reaction, some fundamental aspects of the MEA–CO_2 interaction in aqueous solution remain uncertain.[11–20]

Atomic-level characterization of the complex reaction-diffusion behavior in aqueous solutions appears to be very challenging,

This journal is © the Owner Societies 2015

Phys. Chem. Chem. Phys., 2015, **17**, 831–839 | 831

in part because of the limited capabilities of common instrumentation. A complementary computational effort has been made in studying the fundamental issues related to CO_2 capture and solvent regeneration. The reaction of CO_2 with aqueous amines has often been studied using an implicit solvent approach based on (static) quantum mechanical (QM) calculations;[11–14] the implicit QM model may provide useful insight into the reaction paths and energetics and the relative stability of reaction intermediates. However, there are several less studied aspects like the microstructure of the solvent that may have a critical influence on the MEA–CO_2 reaction. Very recently, *ab initio* molecular dynamics (AIMD) has been applied to identify the likely events and the reaction intermediates involved in the CO_2 capture by MEA.[17–19] This method possibly better accounts for the solution structure and dynamics and their effects on the progress of the reaction, but is limited to small systems. While a quantitative understanding of the CO_2 capture mechanisms is still lacking, the solvent regeneration process that may be the most energy intensive and least understood seems to be forgotten in most of the previous computational studies reported in the literature thus far. In addition, there are relatively few studies investigating how MEA and intermediates behave in bulk solution,[21–24] and little understanding of how they may affect the ability of CO_2 to be captured or the solvent to be regenerated.

In this work, we investigate molecular mechanisms underlying the CO_2 capture by aqueous MEA and the solvent regeneration using combined QM and force field calculations. Using AIMD, we first identify the likely elementary reaction steps and intermediates taking into account the structural and dynamics effects in the MEA–CO_2–H_2O solution. We then use a static quantum chemical approach at the B3LYP/6-311++G level of theory to explain the events observed from AIMD in terms of the reaction energetics and the relative stability of intermediates. Thereafter we use classical molecular dynamics (CMD) to analyze the availability and arrangement of H_2O molecules around amine species, particularly intermediate zwitterions, and discuss its impact on the progress of the MEA–CO_2 reaction. We believe that this effort will help us to better understand the fundamental mechanisms for CO_2 capture and solvent regeneration, which will in turn assist in identifying the factors that could lead to the development of improved solvents.

II. Computational methods

A. Quantum mechanical calculation

We performed AIMD simulations within the Born–Oppenheimer (BO) approximation. The potential energy surfaces for AIMD were generated using density functional theory (DFT) within Perdew–Berke–Ernzerhof generalized gradient approximation[25] (GGA-PBE), as implemented in the Vienna Ab initio Simulation Package[26] (VASP). The projector augmented wave (PAW) method with a planewave basis set was employed to describe the interaction between the core and valence electrons. An energy cutoff of 400 eV was applied for planewave expansion of the electronic eigenfunctions. Only the gamma point was sampled for Brillouin zone integration.

We used the Gaussian 09 program[27] for static QM calculations to investigate the detailed interactions of CO_2 with MEA. Geometry optimizations were performed with hybrid Becke 3-Lee–Yang–Parr (B3LYP) exchange–correlation functional with the 6-311++G basis sets for C, H, N, and O. All stationary points were verified as minima by full Hessian and harmonic frequency calculations. The self-consistent reaction field theory (SCRF) based on the polarisable continuum model (IEFPCM-UFF) implemented in the Gaussian program[28,29] was employed to account for solvation effects implicitly.

B. Classical molecular dynamics simulation

CMD simulations were performed using the Large-scale Atomic/Molecular Massively Parallel Simulator (LAMMPS) program.[30] We used a modified AMBER force field[22,31] for MEA and its derivatives with the SPC/E water model,[32] and obtained the atomic charges for MEA–CO_2 zwitterion, carbamate, and protonated MEA from QM calculations at the B3LYP/6-311++G level of theory; the force field parameters employed are available in ESI.† All the bonds involving H atoms were constrained using the SHAKE algorithm.[33] Spherical cutoffs of 10 Å and 12 Å were used for the Lennard-Jones and Coulomb interactions, respectively. Electrostatic interactions beyond the cutoff were calculated using the Ewald summation method.[34] Simulations were run in the *NVT* ensemble with the temperature controlled by a Nosé–Hoover thermostat[35] with a 100 fs damping parameter. Each simulated system was first annealed at 1000 K and then quenched to 323 K, followed by another anneal and quench cycle. Production runs were carried out for 0.7 ns with a timestep of 1 fs.

III. Results and discussion

A. Elementary reaction steps identified using AIMD

We first attempted to identify the possible elementary steps involved in the reaction of CO_2 with aqueous MEA. The aqueous MEA–CO_2 system has a large number of degrees of freedom and the static approach is often inadequate to accurately describe the complex solution structure and dynamics. AIMD simulations may help identify the likely events and the reaction intermediates; this approach has been proven to be a reliable option for the study of CO_2 absorption and proton transfer in aqueous amine solutions.[17–19]

As presented in Fig. 1, we have identified four likely elementary reaction steps for CO_2 capture:

(a) CO_2 binding with the N of MEA to form the zwitterionic adduct [$MEA + CO_2 \rightarrow MEA^+COO^-$].

(b) Deprotonation by H_2O from the zwitterion to form the carbamate and the solvated proton [$MEA^+COO^- + H_2O \rightarrow MEACOO^- + H_3O^+$].

(c) Abstraction of the solvated proton by another MEA molecule to form the protonated MEA [$MEA + H_3O^+ + MEACOO^- \rightarrow MEAH^+ + H_2O + MEACOO^-$].

(d) Protonation of the O site of carbamate to form the carbamic acid [$MEACOO^- + H_3O^+ \rightarrow MEACOOH + H_2O$]; it is

832 | *Phys. Chem. Chem. Phys.*, 2015, **17**, 831–839
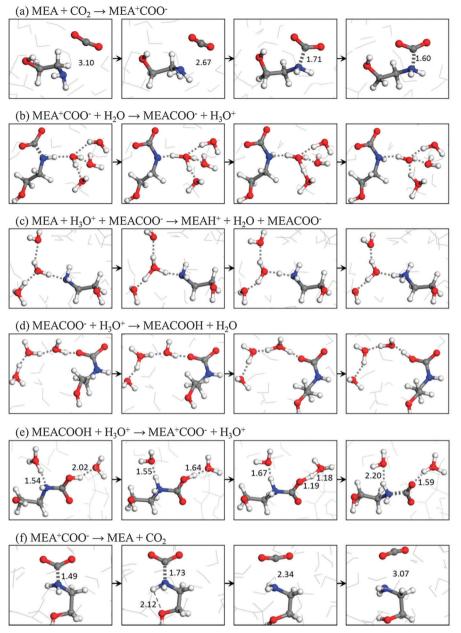
This journal is © the Owner Societies 2015

Fig. 1 AIMD snapshots showing the elementary reaction steps during CO_2 capture in aqueous MEA (a–d) and MEA regeneration (e–f). Distances are given in Å.

found that the proton is subsequently transferred through a water bridge to nearby MEA to form MEAH$^+$.

Looking at reaction (a), the polarized CO_2 in water adopts a bent configuration from its linear shape due to reordering of molecular orbitals (that causes increased charge separation between the C and O atoms, *i.e.*, C becomes slightly more positive). The O–C–O bond angle decreases below 140° while the CO_2 approaches MEA to form a zwitterionic adduct (MEA$^+$COO$^-$). In the zwitterion, the interaction between C (of CO_2) and N (in MEA) seems to be weak as the C–N distance varies between 1.43 Å and 2.11 Å.

Our AIMD simulations were performed using a cubic box of side length 9.278 Å with periodic conditions; each simulation box consists of 2MEA, 1CO_2, and 20H_2O molecules, corresponding to

≈ 25 wt% aqueous MEA solution. The calculated density of 1.095 g cm^{-3} is in reasonable agreement with experiments.[36] We first relaxed the initial structure of system using CMD simulations, and then carried out AIMD simulations at 400 K to examine the reaction of CO_2 with MEA. Here, the relatively high temperature of 400 K was used to speed up the reaction so as to identify possible elementary reactions involved during the limited simulation time span ($\sim$100 ps). As discussed in the following sections, the elementary reactions identified are mainly governed by the arrangement and configuration of the involved species with no significant barriers, rather than the relative heights of activation barriers among possible events. Hence, raising the temperature would be an appropriate way of accelerating the reaction dynamics as it may not significantly alter the ratios of the

This journal is © the Owner Societies 2015

Phys. Chem. Chem. Phys., 2015, **17**, 831–839 | **833**

low-barrier rate constants; nonetheless, to minimize any potential temperature-induced biases, we ran several independent simulations by varying the initial distributions of constituent molecules. The same simulation conditions were employed for the cases (b)–(d).

In reaction (b), the N-bound proton is transferred to the water network through a close-by H_2O molecule; the deprotonation strengthens the C–N bond in the resulting $MEACOO^-$. Our AIMD simulation shows that the deprotonation and the subsequent proton hopping happen rapidly. This suggests that the barrier for the deprotonation process would be insignificant if the local water arrangement allows the strong interaction between the acidic H (in MEA^+COO^-) and O (in H_2O) atoms; indeed, our static QM calculations show that the deprotonation barrier can be less than 0.1 eV, depending on the water arrangement (*vide infra*). These results show the zwitterionic adduct to be the intermediate for the formation of stable carbamate, as also suggested by previous studies.[8,9]

The solvated proton is found to undergo rapid migration following the Grotthuss-like mechanism[37] until it is abstracted by an available basic site such as N in MEA (or $MEACOO^-$) or O in $MEACOO^-$. As shown in Fig. 1(c), the proton binds to the N of MEA giving rise to an ion-pair $[MEAH^+][MEACOO^-]$; this is consistent with previous nuclear magnetic resonance (NMR) studies that show $MEACOO^-$ and $MEAH^+$ to be the major products of CO_2 capture in aqueous MEA.[38]

Our AIMD simulations also show that a proton preferentially binds to the O of $MEACOO^-$, rather than the N site, forming carbamic acid, as illustrated in Fig. 1(d); this is because the O site is more easily accessible by neighboring H_2O molecules, as discussed in Section C. We also find that the proton in MEACOOH tends to be easily released and is eventually abstracted by MEA (if available) to form $MEAH^+$, implying that MEACOOH is another important intermediate, rather than a product.

Fig. 1(e) and (f) show the AIMD snapshots for CO_2 removal from $MEACOO^-$ (MEA regeneration). The simulation was run at 1000 K in order to accelerate the solution dynamics and thus the reaction; the high-temperature AIMD would not significantly bias the reaction, as reasoned earlier. Here, $2MEACOO^-$ molecules, $20H_2O$ molecules, and 3 protons were placed in a cubic box of side length 9.364 Å. We observe the protonation of the N in MEACOOH forms an unstable protonated species followed by deprotonation from the O site to form a relatively more stable MEA^+COO^- [(e)]. Then, as shown in Fig. 1(f), the alkanolamine chain is seen to reconfigure to the ring form, which allows the intramolecular H-bonding interaction between acidic H (in NH_2) and O (in OH), facilitating CO_2 removal. These results highlight how the competition between the intramolecular and intermolecular H-bonding interactions, as determined by the local water arrangement around NH_2, affects the MEA^+COO^- configuration and in turn the relative probability between CO_2 desorption and deprotonation.

We also estimated the reaction energy of CO_2 (ΔE_{rxn}) in 30 wt% aqueous MEA by comparing the total energies of the reacted (E_R) and unreacted (E_U) systems from AIMD simulations (see Fig. S1, ESI†), *i.e.*, $\Delta E_{rxn} = E_R - E_U$. Here, the reacted and unreacted systems consist of ($1MEACOO^-$, $1MEAH^+$, $16H_2O$) and ($2MEA$, $1CO_2$, $16H_2O$), respectively; all simulation boxes were cubic with

side lengths of 8.77 Å and periodic boundary conditions. Our calculations predict ΔE_{rxn} to be -73.33 ± 27.02 kJ mol^{-1} CO_2; although the sizes of the simulation systems are fairly small, the predicted ΔE_{rxn} is in reasonable agreement with the experimentally estimated value of -89 ± 4 kJ mol^{-1} CO_2 in 30 wt% MEA.[39]

B. Static QM analysis of fundamental MEA–CO₂ interactions

In this section, we attempted to address the following fundamental questions raised from the AIMD simulations using static QM calculations.

• What is the driving force for the CO_2 capture by MEA?

• How does the CO_2 binding affect the deprotonation from MEA^+COO^-?

• How does the arrangement of H_2O molecules affect the protonation/deprotonation and CO_2 capture/removal processes?

We analyzed the geometric and electronic structures of MEA and its derivatives and calculated the activation energy barriers for specific protonation/deprotonation reaction steps at the B3LYP/6-311++G level of theory.

The interaction of CO_2 and MEA represents a classical donor–acceptor interaction, wherein, CO_2 is the Lewis acid and MEA is the Lewis base. The anti-bonding (empty) orbital of CO_2 accepts electrons from the lone pair of N in MEA; the non-bonding molecular orbital is calculated to display about 26.84% s character and 73.16% p character in an aqueous system.

As shown in Fig. 2, in the QM study, we mostly considered open chain-like geometry for the considered amine species with two additional H_2O molecules; the explicit H_2O molecules were placed to form hydrogen bonds with the NH_2 and OH functional groups of the amines. When the N and O atoms are exposed to nearby H_2O molecules and form intermolecular H-bonding, the MEA and its derivatives are likely to adopt an open chain configuration to maximize the intermolecular H-bonding interactions. Note that, in contrast to this, if the water arrangement does not allow intermolecular H-bonding, the alkanolamine molecules attain stability by adopting a ring-like form which facilitates the intramolecular H-bonding interaction between N (or H) in NH_2 and H (or O) in OH.

In the MEA–CO_2 zwitterion (MEA^+COO^-), the distance between C (of CO_2) and N (of MEA) is predicted to be 1.608 Å with a C–N vibrational frequency of 692.71 cm^{-1}. Note that the calculated vibrational frequency is somewhat perturbed by neighboring bonds, but the information is useful in understanding the nature of C–N interaction; in this case, the C–N bond is much weaker than a single C–N bond that typically shows a frequency greater than 1100 cm^{-1}. Once the C–N interaction is established, the N–H interaction is weakened with a concurrent depopulation of Π_{NH_2} bonding orbitals that may facilitate deprotonation ($MEA^+COO^- \rightarrow MEACOO^- + H^+$).[40]

Considering a simplistic picture, wherein the Π_{NH_2} orbital is obtained by a constructive combination of the H 1s and N 2p orbitals, our QM calculation predicts the gross population of the Π_{NH_2} orbital to reduce to 2.839 in MEA^+COO^- (from the 2.957 in MEA). In addition, natural bond order analysis was carried out using single points calculations with STO-3G basis set after the geometric optimization with B3LYP/6-311++G.
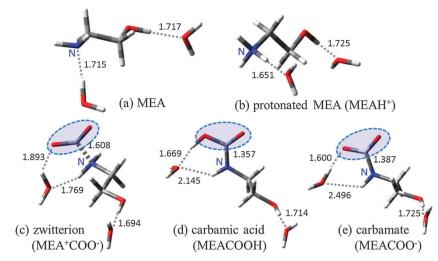
834 | *Phys. Chem. Chem. Phys.*, 2015, **17**, 831–839

This journal is © the Owner Societies 2015

Fig. 2 Optimized geometries of MEA and its derivatives with two explicit H_2O molecules using QM calculations at a theory level of B3LYP/6-311++G. The white, grey, blue, and red represent H, C, N, and O atoms, respectively. Selected bond distances are given in Å.

We obtained the following orbital coefficients and hybridizations for the two N–H bonding orbitals in MEA and MEA^+COO^-:

MEA: (1) 0.7715 N $sp^{3.06}$ + 0.6363 H s and

(2) 0.7718 N $sp^{3.05}$ + 0.6359 H s

MEA^+COO^-: (1) 0.7895 N $sp^{3.06}$ + 0.6138 H s and

(2) 0.8090 N $sp^{2.74}$ + 0.5858 H s.

In MEA, the coefficients corresponding to (1) and (2) are almost identical. Note that the slight difference in values results from the different orientation of H atoms (in NH_2) with respect to the OH group and the intermolecular H-bonding between N (of MEA) and H of (H_2O). On the other hand, in MEA^+COO^-, the N contribution in (2) is higher than (1) by 3.13%, indicating that the N–H(2) bond is more N-like and the acidic H may undergo relatively easy deprotonation.

MEA^+COO^- is also reported to react with OH^- (or H_2O) and form bicarbonate (HCO_3^-), but carbamate ($MEACOO^-$) and carbamic acid (MEACOOH) may be more likely to form,[17] as also shown earlier in our AIMD simulations [Fig. 2(d) and (e)]. The C–N distance of 1.39 Å in $MEACOO^-$ is similar to 1.36 Å in MEACOOH, however a lower C–N vibrational frequency of 1280 cm^{-1} (compared to 1578 cm^{-1} in MEACOOH) suggests that $MEACOO^-$ yields a greater single bond like character; the predicted frequency value shows excellent agreement with the experimental value of 1322 cm^{-1} (ref. 39). Another important product is protonated MEA ($MEAH^+$) [Fig. 2(b)]. After deprotonation from MEA^+COO^-, the proton hopping through water bridges can facilitate proton abstraction by another MEA molecule.

Next, we estimated the relative binding strengths of proton and CO_2 in MEA^+COO^- using the following formulas.

$$E_b(H^+) = E_M + E_{H^+} - E_{H^+/M} \qquad (1)$$

$$E_b(CO_2) = E_M + E_{CO_2} - E_{CO_2/M} \qquad (2)$$

where $E_{H^+/M}$ and $E_{CO_2/M}$ represent the total energies of the protonated and CO_2 bound species, respectively, E_M is for the species before proton/CO_2 binding, and E_{H^+} and E_{CO_2} are the energies of solvated proton and gas-phase CO_2, respectively. Here, E_{H^+} was calculated considering the difference in energies between a system with pure H_2O (5 molecules) and a system with one H_3O^+ molecule and 4 water molecules; to verify the proton solvation energy, we also considered a system with $H_5O_2^+$ cluster formation and the energy turned out to be similar. E_{H^+} is predicted to be 279 kcal mol^{-1}, very close to the experimental value of 270 kcal mol^{-1}.[41]

Predicted $E_b(H^+)/E_b(CO_2)$ values are found to be sensitive to the H-bonding interactions in the system, as shown in Fig. 3. When considering a continuum implicit solvent model with no explicit H_2O molecule, for the open-chain configuration [(a)], $E_b(CO_2)$ is predicted to be 0.38 eV while $E_b(H^+)$ is significantly lower with a value of 0.19 eV; on the other hand, in the ring form [(b)], predicted $E_b(CO_2)$ and $E_b(H^+)$ values are 0.49 eV and 0.36 eV, respectively. The significant differences in E_b between the ring and open-chain configurations may stem from the additional intramolecular H-bonding interaction between H(1) (in NH_2) and O (in OH) in the ring form, as shown in Fig. 3(b); the resulting weakening of the N–H(1) bond in turn strengthens the N–H(2) and N–C (of CO_2) bindings.

As summarized in Fig. 4, for various configurations (see ESI†), we also calculated and compared the proton binding strengths at N in MEA (denoted as N_M) and N in $MEACOO^-$ (N_C). The lower $E_b(H^+)$ at the N_C site relative to the N_M site suggests the relative ease of deprotonation from MEA^+COO^-. In addition, we find that the deprotonation barrier can be insignificant provided the proton is linked to a well-connected water network; as shown in Fig. S3 (ESI†), our value of 0.08 eV is much smaller than 0.26–0.35 eV as recently reported by Guido et al.,[18] most likely due to different water arrangements around the amine species considered. We also consider direct proton transfer from MEA^+COO^- to a nearby MEA, which turns out to be very facile with a negligible barrier provided they are in the
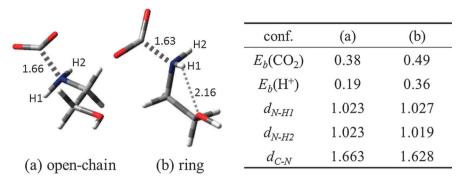
conf.	(a)	(b)
$E_b(CO_2)$	0.38	0.49
$E_b(H^+)$	0.19	0.36
$d_{N\text{-}H1}$	1.023	1.027
$d_{N\text{-}H2}$	1.023	1.019
$d_{C\text{-}N}$	1.663	1.628

Fig. 3 Predicted relative binding energies (in eV) of CO_2 [$E_b(CO_2)$] and H^+ [$E_b(H^+)$] in the open-chain [(a)] and ring [(b)] forms of zwitterion (MEA^+COO^-). The white, grey, blue, and red represent H, C, N, and O atoms, respectively. Selected bond distances are given in Å.
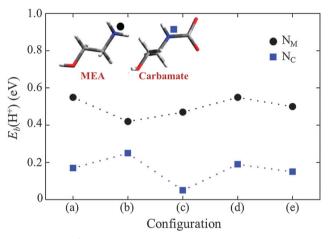

Fig. 4 Relative H^+ binding energies (in eV) at N in MEA and N in carbamate ($MEACOO^-$), denoted as N_M and N_C, respectively, for five different configurations (ESI†).

right orientation (see Fig. S4, ESI†); however, solvation of MEA^+COO^- is more likely in the 30 wt% MEA solution.

To better understand the key role played by neighboring H_2O molecules in facilitating proton transfer, we calculated the activation barriers for the proton transfer from one abstraction site to another mediated by one and two H_2O molecules, as displayed in Fig. 5. For the proton transfer from the N to the O

atom in MEA^+COO^-, the activation barrier is substantially reduced from 0.67 eV to 0.40 eV as the process is mediated by two H_2O molecules [(b)], compared to the case with one H_2O molecule [(a)]. This result clearly demonstrates that the local arrangement of H_2O molecules may play a critical role in determining the protonation/deprotonation processes, although the simple model systems considered may not represent the complex reaction dynamics in the aqueous MEA–CO_2 system. This warrants more systematic investigations regarding the influence of local water arrangement around amine species on the reaction of CO_2 with aqueous amines; in the following section, we will attempt to touch on this issue rather briefly.

C. Effect of solvation environment in reaction progression studied using CMD

As seen from the above AIMD simulations, proton transfer may mainly occur through water bridges in the aqueous solvent. It is therefore expected that the arrangement of H_2O molecules around the basic N and O atoms, in addition to the proton binding energies at the base sites, will be an important factor in determining which sites are preferentially protonated.

The spatial arrangement of H_2O molecules around each protonation or deprotonation site was evaluated by calculating radial distribution functions (RDF) for selected pairs of atoms. Here, we considered N in MEA (denoted as N_M), N in $MEACOO^-$ (N_C), and O of the CO_2 moiety in $MEACOO^-$ (O_C), and their
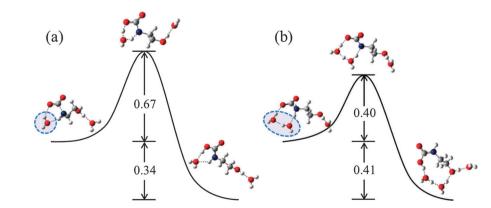

Fig. 5 Predicted pathways and energetics (in eV) for proton transfer from the N to the O site (of the CO_2 moiety) in zwitterion (MEA^+COO^-) via (a) one H_2O molecule and (b) two H_2O molecules as indicated. The white, grey, blue, and red balls represent H, C, N, and O atoms, respectively.
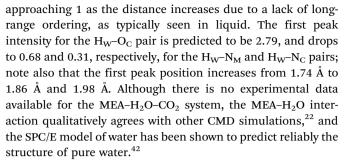
pairwise interactions with H in H_2O (H_W) to assess the protonation processes. Similarly, to understand the deprotonation reactions, we also looked at the pairwise interactions between acid H in $MEAH^+$ ($H_{N,PM}$) [or MEA^+COO^- ($H_{N,ZI}$)] and O in H_2O (O_W).

In this work, two systems of different composition were taken into account to examine how the pairwise interactions will vary with the progress of the CO_2 capture by MEA. System 1 consists of 182MEA and 1517H_2O molecules in a 40 × 40 × 40 $Å^3$ simulation box with periodic boundary conditions, corresponding to approximately 30 wt% aqueous MEA. System 2 contains 10MEA, 86$MEAH^+$, 86$MEACOO^-$, and 1517H_2O molecules in the same simulation box size, assuming that the aqueous MEA solution captures CO_2 to nearly 50% absorption capacity. In both systems, 10 additional MEA^+COO^- intermediates were added; the model systems may not represent all possible composition variations during actual processing, but should be sufficient for understanding the influence of composition on the local arrangement of H_2O molecules around MEA and its derivatives.

Fig. 6 shows the RDF profiles for the H_W–N_M, H_W–N_C and H_W–O_C pairs in System 2 based on the CMD results at 323 K. The inset compares the $g(H_W$–$N_M)$ between System 1 and System 2. $g(r)$ was averaged from trajectories generated every 2 ps according to the following equation where $n(r, r + dr)$ is the number of atoms in a spherical shell of radius r (from the reference atom) and thickness of dr and ρ is the bulk number density.

$$g(r) = \left\langle \frac{n(r, r + dr)}{4\pi r^2 \rho \, dr} \right\rangle$$

All RDFs exhibit a distinct peak at a distance around 2 Å, due to the H-bonding interaction with the nearest H_2O neighbors,

approaching 1 as the distance increases due to a lack of long-range ordering, as typically seen in liquid. The first peak intensity for the H_W–O_C pair is predicted to be 2.79, and drops to 0.68 and 0.31, respectively, for the H_W–N_M and H_W–N_C pairs; note also that the first peak position increases from 1.74 Å to 1.86 Å and 1.98 Å. Although there is no experimental data available for the MEA–H_2O–CO_2 system, the MEA–H_2O interaction qualitatively agrees with other CMD simulations,[22] and the SPC/E model of water has been shown to predict reliably the structure of pure water.[42]

The higher intensity and closer position of the first peak of $g(H_W$–$O_C)$ suggests that the terminal O_C atoms are more likely to form H bonds with neighboring H_2O molecules, compared to the N_C and N_M atoms, and thus kinetically they can more easily abstract H^+ from the protonated water network. The significant reduction in the first peak intensity of $g(H_W$–$N_C)$, in comparison to $g(H_W$–$N_M)$, is primarily due to the bound COO^- attracting H_2O molecules that would otherwise be interacting with N_C. As shown in the inset of Fig. 6, we also find that there is no significant change between System 1 and System 2 for $g(H_W$–$N_M)$, suggesting that the interaction of N_M with neighboring H_2O molecules is not strongly affected by varying amine composition at different stages of the CO_2 absorption process.

Fig. 7 shows the RDFs for the atom pairs of O_W–$H_{N,PM}$, O_W–$H_{N,ZI}$, and O_W–$H_{N,M}$ in System 2; here, $H_{N,M}$ indicates an H atom in the NH_2 functional group of MEA, which is included for comparison. The first peak intensities for the O_W–$H_{N,PM}$, O_W–$H_{N,ZI}$, and O_W–$H_{N,M}$ cases are estimated to be 1.27, 1.08, and 0.62, respectively; the peak positions correspondingly increase from 1.86 Å to 1.98 Å and 2.22 Å. According to the RDF analysis, the H_N atoms of both $MEAH^+$ and MEA^+COO^- are likely to more strongly interact with neighboring H_2O
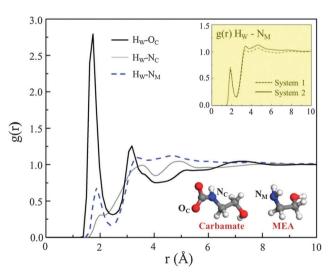
Fig. 6   Radial distribution functions between H of H_2O (H_W) and N_M, O_C, N_C in System 2. Inset is radial distribution function for atom pair H_W–N_M in System 1 and System 2, from MD simulations performed at 323 K. System 1 consists of 182MEA, 10MEA^+COO^-, and 1517H_2O molecules and System 2 contains 10MEA, 10MEA^+COO^-, 86$MEAH^+$, and 86$MEACOO^-$, and 1517H_2O molecules in a 40 × 40 × 40 $Å^3$ simulation box with periodic boundary conditions; this corresponds to approximately 30 wt% aqueous MEA.
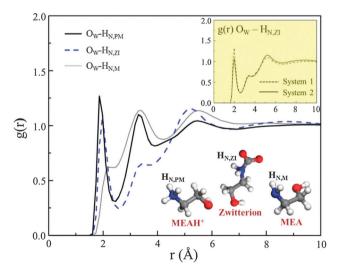
Fig. 7   Radial distribution functions between O of H_2O (O_W) and $H_{N,ZI}$, $H_{N,PM}$ and $H_{N,M}$ in System 2, from MD simulations at 323 K. Inset shows a comparison of $g(r)$ for atom pair O_W–$H_{N,ZI}$ between System 1 and System 2. System 1 consists of 182MEA, 10MEA^+COO^-, and 1517H_2O molecules and System 2 contains 10MEA, 10MEA^+COO^-, 86$MEAH^+$, and 86$MEACOO^-$, and 1517H_2O molecules in a 40 × 40 × 40 $Å^3$ simulation box with periodic boundary conditions; this corresponds to approximately 30 wt% aqueous MEA.

molecules compared to the MEA case, which is not surprising considering the more positively charged $H_{N,PM}$ and $H_{N,ZI}$ than the $H_{N,M}$. This result also suggests that deprotonation of MEAH$^+$ may be more kinetically favorable than that of MEA$^+$COO$^-$, albeit insignificant; note that $H_{N,PM}$ is freely exposed to surrounding H_2O molecules while $H_{N,ZI}$ is somewhat shielded by COO$^-$. However, considering the substantially smaller $E_b(H^+)$ at N_C compared to N_M (as shown in Fig. 4), we can expect that deprotonation from MEA$^+$COO$^-$ will be more facile than the MEAH$^+$ case.

From the inset of Fig. 7 which compares $g(O_W–H_{N,ZI})$ in System 1 and System 2, we can see a noticeable decrease in the first peak intensity from 1.33 (System 1) to 1.08 (System 2). This suggests that, as the reaction of MEA with CO_2 proceeds and thus more MEAH$^+$ and MEACOO$^-$ are generated, the charged products tend to attract H_2O molecules, which in turn suppresses the H-bonding interaction between the $H_{N,ZI}$ and O_W atoms. As a consequence, the likelihood of MEA$^+$COO$^-$ deprotonation to the H-bonded water network decreases.

As the H-bonding interaction with surrounding H_2O molecules dwindles, MEA$^+$COO$^-$ tends to be stabilized by forming an intramolecular hydrogen bond between $H_{N,ZI}$ and $O_{H,ZI}$ (of the OH group). The increased intramolecular H-bonding interaction suppresses deprotonation while enhancing CO_2 removal from MEA$^+$COO$^-$, thereby facilitating MEA regeneration. Our study highlights the importance of the availability and arrangement of H_2O molecules, particularly around the zwitterionic intermediate, in the progression of competing CO_2 capture and MEA regeneration processes.

IV. Summary

We examined molecular mechanisms underlying the reaction of aqueous MEA with CO_2 using a combination of quantum mechanical and classical force field calculations, with particular attention to the structural and dynamics effects in the MEA–CO_2–H_2O solution. First, DFT-based AIMD was employed to identify key elementary reactions and intermediates. The simulation results clearly demonstrate that MEA reacts with CO_2 to form a zwitterionic intermediate. The zwitterion is found to undergo deprotonation predominantly by a close-by H_2O molecule in 25 wt% aqueous MEA considered. The solvated proton undergoes rapid migration following the Grotthuss-like mechanism until abstracted by MEA (or carbamate) to form protonated MEA (or carbamic acid); the proton in carbamic acid tends to be easily released and is eventually abstracted by MEA (if available). We also found that carbamate may revert to the zwitterionic state by grabbing a proton. More interestingly, CO_2 tends to be released from the zwitterion, rather than deprotonation, if the acidic H (in NH_2) forms an intramolecular H-bond with O (in OH) instead of interacting with nearby H_2O molecules. Our AIMD results suggest that the competing intramolecular and intermolecular H-bonding interactions, as determined by the availability and arrangement of H_2O molecules around the zwitterion, directly impact the relative probability between CO_2 removal (MEA regeneration) and deprotonation (carbamate formation).

Next, we performed static quantum chemical calculations at the B3LYP/6-311++G level of theory to analyze in more detail the fundamental interactions involved in the MEA–CO_2 reaction. Our analysis of vibration frequencies and gross orbital populations unequivocally demonstrates that CO_2 is bound to MEA by forming a relatively weak C–N bond (compared to a C–N single bond); the CO_2 binding causes a significant weakening of the N–H interaction, which may in turn facilitate deprotonation from the zwitterionic intermediate. The CO_2 and proton binding energies in the zwitterion tend to be lower when it is in the open-chain relative to the ring configuration; in addition, the proton binding strengths at the different basic sites of MEA and carbamate are found to be sensitive to their configurations (which are mainly determined by the competing intramolecular and intermolecular H-bonding interactions). Our calculation also shows that the energy barriers for proton transfer can be significantly altered by the local arrangement of H_2O molecules.

Finally, we evaluated the spatial arrangement of H_2O molecules around MEA and its derivatives by calculating pairwise RDFs using CMD simulations. In particular, we looked at the pairwise interactions of H(O) in H_2O with basic N/O (acidic H) in MEA or carbamate (protonated MEA or zwitterion) to assess the protonation (deprotonation) processes, assuming that proton transfer primarily occurs through water bridges in the aqueous solvent as seen from our AIMD simulations. The results clearly show that the RDFs vary significantly for the different sites considered. For instance, the O of carbamate is more likely to be H-bonded with H_2O, and thus is more kinetically favored for protonation than the N of MEA (or carbamate), consistent with the trend observed in AIMD. We also found that the acidic H of zwitterion interacts less with the O of H_2O, as the reaction progresses and more charged products (such as protonated MEA and carbamate) are present; this may in turn lead to an increase in the intramolecular H-bonding interaction, thereby expectably suppressing deprotonation while enhancing CO_2 removal from the zwitterion. This study highlights the critical role of H_2O molecules, particularly their availability and arrangement around zwitterions, in the progression of competing CO_2 capture and MEA regeneration processes. This also suggests that an explicit description of the solution structure and dynamics on the atomic level would be crucial for elucidating the underlying mechanisms of CO_2 reaction with aqueous amines.

References

1 E. J. Maginn, *J. Phys. Chem. Lett.*, 2010, **1**, 3478–3479.

2 G. T. Rochelle, *Science*, 2009, **325**, 1652–1654.

3 M. Wang, A. Lawal, P. Stephenson, J. Sidders and C. Ramshaw, *Chem. Eng. Res. Des.*, 2011, **89**, 1609–1624.

4 D. Zhu, M. Fang, Z. Lv, Z. Wang and Z. Luo, *Energy Fuels*, 2012, **26**, 147–153.

5 R. E. Dugas and G. T. Rochelle, *J. Chem. Eng. Data*, 2011, **56**, 2187–2195.

6 H. Dang and G. T. Rochelle, *Sep. Sci. Technol.*, 2003, **38**, 337–357.

7 G. S. Goff and G. T. Rochelle, *Ind. Eng. Chem. Res.*, 2004, **43**, 6400–6408.

8 M. Caplow, *J. Am. Chem. Soc.*, 1968, **90**, 6795–6803.

9 P. V. Danckwerts, *Chem. Eng. Sci.*, 1979, **34**, 443–446.

10 J. E. Crooks and J. P. Donnellan, *J. Chem. Soc., Perkin Trans. 2*, 1989, 331–333.

11 H.-B. Xie, Y. Zhou, Y. Zhang and J. K. Johnson, *J. Phys. Chem. A*, 2010, **114**, 11844–11852.

12 E. F. da Silva and H. F. Svendsen, *Ind. Eng. Chem. Res.*, 2004, **43**, 3413–3418.

13 B. Arstad, R. Blom and O. Swang, *J. Phys. Chem. A*, 2007, **111**, 1222–1228.

14 J.-G. Shim, J.-H. Kim, Y. H. Jhon, J. Kim and K.-H. Cho, *Ind. Eng. Chem. Res.*, 2009, **48**, 2172–2178.

15 K. Iida and H. Sato, *J. Phys. Chem. B*, 2012, **116**, 2244–2248.

16 Y. H. Jhon, J.-G. Shim, J.-H. Kim, J. H. Lee, K.-R. Jang and J. Kim, *J. Phys. Chem. A*, 2010, **114**, 12907–12913.

17 B. Han, C. Zhou, J. Wu, D. J. Tempel and H. Cheng, *J. Phys. Chem. Lett.*, 2011, **2**, 522–526.

18 C. A. Guido, F. Pietrucci, G. A. Gallet and W. Andreoni, *J. Chem. Theory Comput.*, 2013, **9**, 28–32.

19 K. Z. Sumon, A. Henni and A. L. L. East, *J. Phys. Chem. Lett.*, 2014, **5**, 1151–1156.

20 Y. Matsuzaki, H. Yamada, F. A. Chowdhury, T. Higashii and M. Onoda, *J. Phys. Chem. A*, 2013, **117**, 9274–9281.

21 Y. S. Yu, H. F. Lu, G. X. Wang, Z. X. Zhang and V. Rudolph, *J. Chem. Eng. Data*, 2013, **58**, 1429–1439.

22 E. F. da Silva, T. Kuznetsova, B. Kvamme and K. M. Merz Jr., *J. Phys. Chem. B*, 2007, **111**, 3695–3703.

23 A. V. Gubskaya and P. G. Kusalik, *J. Phys. Chem. A*, 2004, **108**, 7165–7178.

24 R. López-Rendón, M. A. Mora, J. Alejandre and M. E. Tuckerman, *J. Phys. Chem. B*, 2006, **110**, 14652–14658.

25 J. P. Perdew, K. Burke and M. Ernzerhof, *Phys. Rev. Lett.*, 1996, **77**, 3865–3868.

26 G. Kresse and J. Furthmüller, *Phys. Rev. B: Condens. Matter Mater. Phys.*, 1996, **54**, 11169–11186.

27 M. J. Frisch, G. W. Trucks, H. B. Schlegel, G. E. Scuseria, M. A. Robb, J. R. Cheeseman, G. Scalmani, V. Barone, B. Mennucci, G. A. Petersson, H. Nakatsuji, M. Caricato, X. Li, H. P. Hratchian, A. F. Izmaylov, J. Bloino, G. Zheng, J. L. Sonnenberg, M. Hada, M. Ehara, K. Toyota, R. Fukuda, J. Hasegawa, M. Ishida, T. Nakajima, Y. Honda, O. Kitao, H. Nakai, T. Vreven, J. A. Montgomery, J. E. Peralta, F. Ogliaro, M. Bearpark, J. J. Heyd, E. Brothers, K. N. Kudin, V. N. Staroverov, T. Keith, R. Kobayashi, J. Normald, K. Raghavachari, A. Rendell, J. C. Burant, S. S. Iyengar, J. Tomasi, M. Cossi, N. Rega, J. M. Millam, M. Klene, J. E. Knox, J. B. Cross, V. Bakken, C. Adamo, J. Jaramillo, R. Gomperts, R. E. Stratmann, O. Yazyev, A. J. Austin, R. Cammi, C. Pomelli, J. W. Ochterski, R. L. Martin, K. Morokuma, V. G. Zakrzewski, G. A. Voth, P. Salvador, J. J. Dannenberg, S. Dapprich, A. D. Daniels, O. Farkas, J. B. Foresman, J. V. Ortiz, J. Cioslowski and D. J. Fox, *Gaussian09 Revision C.01*, Gaussian, Inc., Wallingford CT, 2010.

28 J. Tomasi, R. Cammi, B. Mennucci, C. Cappelli and S. Corni, *Phys. Chem. Chem. Phys.*, 2002, **4**, 5697–5712.

29 M. Cossi, G. Scalmani, N. Rega and V. Barone, *J. Chem. Phys.*, 2002, **117**, 43–54.

30 S. J. Plimpton, *J. Comput. Phys.*, 1995, **117**, 1–19.

31 W. D. Cornell, P. Cieplak, C. I. Bayly, I. R. Gould, K. M. Merz Jr., D. M. Ferguson, D. C. Spellmeyer, T. Fox, J. W. Caldwell and P. A. Kolmman, *J. Am. Chem. Soc.*, 1995, **117**, 5179–5197.

32 H. J. C. Berendsen, J. R. Grigera and T. P. Straatsma, *J. Phys. Chem.*, 1987, **91**, 6269–6271.

33 J.-P. Ryckaert, G. Ciccotti and H. J. C. Berendesen, *J. Comput. Phys.*, 1977, **23**, 327–341.

34 U. Essmann, L. Perera, M. L. Berkowitz, T. Darden, H. Lee and L. G. Pedersen, *J. Chem. Phys.*, 1995, **103**, 8577–8593.

35 W. G. Hoover, *Phys. Rev. A: At., Mol., Opt. Phys.*, 1985, **31**, 1695–1697.

36 R. H. Weiland, J. C. Dingman, D. B. Cronin and G. J. Browning, *J. Chem. Eng. Data*, 1998, **43**, 378–382.

37 C. J. T. Grotthuss, *Ann. Chim.*, 1806, **58**, 54–73.

38 G. Fan, A. G. H. Wee, R. Idem and P. Tontiwachwuthikul, *Ind. Eng. Chem. Res.*, 2009, **48**, 2717–2720.

39 H. Arcis, K. Ballerat-Busserolles, L. Rodier and J. Y. Coxam, *J. Chem. Eng. Data*, 2011, **56**, 3351–3362.

40 A. K. Chakraborty, K. B. Bischoff, G. Astarita and J. R. Damewood, *J. Am. Chem. Soc.*, 1988, **110**, 6947–6954.

41 F. Khalili, A. Henni and A. L. L. East, *J. Mol. Struct.: THEOCHEM*, 2009, **926**, 1–9.

42 P. Mark and L. Nilsson, *J. Phys. Chem. A*, 2001, **105**, 9954–9960.

This journal is © the Owner Societies 2015

Phys. Chem. Chem. Phys., 2015, **17**, 831–839 | **839**